Long-term exposure to elevated pCO_2 more than warming modifies early-life shell growth in a temperate gastropod

List of Authors: Saskia Rühl[1,2]*, Piero Calosi[2,3], Sarah Faulwetter[4], Kleoniki Keklikoglou[4], Stephen Widdicombe[1], Ana M Queirós[1]*

[1 2]Plymouth Marine Laboratory, Prospect Place, West Hoe, Plymouth, PL1 3DH, UK.

[2]Marine Biology and Ecology Research Centre, School of Marine Science and Engineering, Davy Building, Plymouth University, Drake Circus, Plymouth, Devon, PL4 8AA, UK

[3]Département de Biologie, Chimie et Géographie, Université du Québec à Rimouski, 300 Allée des Ursulines, Rimouski, QC G5L 3A1, Canada

[4] Institute of Marine Biology, Biotechnology and Aquaculture, Hellenic Centre for Marine Resarch, Thalassocosmos, 71500 Heraklion, Crete, Greece4)

*Corresponding Authors: Saskia Rühl: saskia.ruehl@freenet.de, 07932529890

Ana Queirós: anqu@pml.ac.uk, 01752 633100

Abstract

Co-occurring global change drivers, such as ocean warming and acidification, can have large impacts on the behaviour, physiology and health of marine organisms. However, whilst early-life stages are thought to be most sensitive to these impacts, little is known about the individual level processes by which such impacts take place. Here, using mesocosm experiments simulating ocean warming (OW) and ocean acidification (OA) conditions expected for the NE Atlantic region by 2100 using a variety of treatments of elevated pCO_2 and temperature. We investigated their impacts on bio-mineralisation, microstructure and ontogeny of *Nucella lapillus* (L.) juveniles, a common gastropod predator that exerts important top-down controls on biodiversity patterns in temperate rocky shores. The shell of juveniles hatched in mesocosms during a 14 month long experiment were analysed using micro-CT scanning, 3D geometric morphometrics and scanning-electron microscopy. Elevated temperature and age determined shell density, length, width, thickness, elemental chemistry, shape and shell surface damages. However, co-occurring elevated pCO_2 modified the impacts of elevated temperature, in line with expected changes in carbonate chemistry driven by temperature. Young *N. lapillus* from acidified treatments had weaker shells and were therefore expected to be more vulnerable to predation and environmental pressures such as wave action. However, in some instances, the effects of both higher CO_2 content and elevated temperature appeared to have reversed as the individuals aged. This study suggests that compensatory development may therefore occur, and that expected increases in juvenile mortality under OA and OW may be counteracted, to some degree, by high plasticity in shell formation in this species. This feature may prove advantageous for *N. lapillus* community dynamics in near-future conditions.

Keywords: Climate change; CT scanning; Early-life stage; Electron microscopy; Juvenile; Mollusc; Ocean acidification; Ocean warming

44

Introduction

Many marine organisms have evolved external shells that provide protection against predation, desiccation and other inhospitable abiotic factors, and prevent parasitism (Brusca & Brusca 2003). A damage or loss of shell-mass therefore diminishes the organism's likelihood of survival (Parker *et al.* 2013). Marine external shells are most frequently composed of a number of carbonated forms including minerals such as calcium and magnesium, as well as organic coatings (Vermeij 1995).

Calcium carbonate ($CaCO_3$) is the most common material in marine shells and can occur in several forms with different chemical and mechanical properties (Weiss *et al.* 2002). Shell $CaCO_3$ composites are arranged in layers of varying complexity, each consisting of a different form of $CaCO_3$ (Falini *et al*. 1996). Aragonite and calcite are the two most common $CaCO_3$ forms (Suzuki & Nagasawa 2013). Calcite is more structurally diverse and more stable but requires comparatively more time and energy to be produced than aragonite (Weiss *et al.* 2002). Calcite is also mechanically weaker, and more resistant to corrosive effects of low pH environments than aragonite, typically forming trigonal-rhombohedrally shaped crystals, (Weiss *et al.* 2002). Conversely, aragonite occurs in orthorhombic acicular crystals, often appearing in parallel layers. Both materials vary in seawater solubility according to variations in ocean carbonate chemistry and temperature (Plummer & Busenberg 1982,). For instance, CO_2 driven acidification can cause reductions in $CaCO_3$ saturation, making calcification more energetically costly for individuals relying on aragonite and calcite (Feely *et al*. 2004). Under-saturation of $CaCO_3$ therefore increases the risk of fast rates of shell dissolution, at which recovery may not take place (Nienhuis *et al.* 2010). In addition, seawater magnesium carbonate ($MgCO_3$) may also become under-saturated because of carbonate chemistry changes in seawater. The magnesium: calcium (Mg^{2+}:Ca^{2+}) ratio in seawater influences organic calcification processes on a microscopic level, so acidification can tip calcification towards the deposition of specific forms (Ries 2010). Low levels of Mg^{2+} favour the formation of calcite, and high levels favour the deposition of aragonite (Ries 2010). Juvenile

molluscs preferentially deposit aragonite, possibly due to weaker controls over the early bio-mineralisation processes (Weiss 2002), and on approaching maturity, calcite deposition increases. Differences in mineralisation over the individual life cycle can therefore lead to higher mortality in juveniles due to predation or parasitism, because shells are not yet as stable nor as thick as in adults. These shells are also thought to dissolve more easily in conditions of lowered pH, especially in or just after the settling process (Green *et al*. 2004). Such conditions have been found increasingly often in marine environments around the world as a consequence of global climate change.

Changes in seawater temperature (i.e. ocean warming, "OW") and in carbonate chemistry and pH driven by increasing CO_2 emissions (i.e. ocean acidification, "OA") (IPCC 2014) are known to impact the integrity and morphology of the shell of adult marine organisms (Nienhuis *et al*. 2010, Thompsen *et al*. 2010, Melatunan *et al*. 2013). Some defence mechanisms such as decreased shell growth rates to preserve energy (Findlay *et al*. 2010) and increased calcification in a range of calcifying species across taxa have been observed in acidified conditions (Ries *et al.* 2009). However, whilst we have a good understanding of OW and OA impacts on adult shell bearing organisms, our current understanding of how the same stressors and their interactions may impact embryos and juveniles is still limited (Byrne and Przelawsky 2013, Kurihara 2008, Melatunan *et al.* 2013, Sanford *et al.* 2014). The energetic implications of dealing with multiple stressors can cause a reduction and/or reallocation of an organism's energy budget (Melzner *et al*. 2013) such that trade-offs among different homeostatic processes caused by a given stressor can reduce the individual's ability to cope with another stressor (*e.g.* Calosi *et al.* 2013). These interactions can lead to complex changes at the individual-level and in species interactions, affecting the natural structuring of biological communities (Queirós *et al*. 2015). As the survival of populations depends on the survival of their offspring (Widdicombe & Spicer 2008), early-life stages (e.g. Dupont & Thorndyke 2009), on transgenerational responses (e.g. Sunday *et al*. 2014)

and species interactions are therefore needed to scale up population and community level responses to climate change and OA (Reusch 2014, Sunday *et al*. 2014).

This study aimed to quantify the combined effects of OW and OA as simulated through elevated CO_2 content and temperature treatments, on the shell development and growth of the juveniles of the temperate marine gastropod *Nucella lapillus* (Linnaeus 1758), a predator that exerts important top-down controls on the biodiversity of North Atlantic temperate rocky shores (Trussel *et al*. 2003). *Nucella lapillus* (hereafter "*N. lapillus*") is an abundant species in temperate shores of the North Atlantic that exhibits a certain phenotypic plasticity in shell morphology and colour depending on latitude, microhabitat, physiological stress, and mechanical stresses such as those caused by wave actions and predation. *N. lapillus* is a direct developer that predates on habitat forming species such as barnacles and mussels, and has a great influence on benthic community structure and dynamics, habitat complexity and diversity (Trussel *et al*. 2003, Sanford *et al*. 2014). In this study, shell length, width, thickness, density, crystallisation, chemical make-up and overall shapes of juveniles from different treatment combinations, at three and nine weeks post hatching, were examined. Animals were collected over a 14 month mesocosm experiment featuring multiple combinations of elevated CO_2 content and temperature treatments (simulating various scenarios of OA and OW projected for the end to the 21st century in the region), during which marked effects of both stressors were observed in adult *N. lapillus* energetics and shell structure (Queirós *et al*. 2015). Considering that *N. lapillus* is a direct developer, we expected that if no phenotypic adjustment occurred during embryonic and post-hatching ontogeny, juveniles hatched during the experiment would develop shells with significant changes in growth patterns and chemistry, reflecting impacts observed in the parental lineage. However, if developmental acclimatisation was to occur, we expect no significant changes to be observed at the levels of shell, as phenotypic buffering could favour the maintenance of this ecologically and physiologically important structure.

Material and Methods

Specimen acquisition

Juveniles of *N. lapillus* were collected during the NERC-DECC UK Ocean Acidification Research Programme's mesocosm experiments (Queirós *et al.* 2015), carried out at Plymouth Marine Laboratory's Intertidal Mesocosm Acidification System (PML-IMAS, Findlay *et al.* 2013) during 2011-2012. Mature individuals from a native population at Mouth Batten, Plymouth (N50° 21' 30.29", E -4° 7' 50.07") were collected and transferred to the PML-IMAS where they were exposed to five different treatments combining various temperature and pCO_2 levels for 14 months (Queiros *et al.* 2015). During the experiment, the offspring hatched from egg capsules laid in the mesocosm were maintained in this system, and analysed in the present study. A detailed description of the set-up, carbonate chemistry parameters and of how the experimental treatments were controlled can be found in Queirós *et al.* (2015). Briefly, five treatments combining seawater pCO_2 (380, 750 and 1000 ppm) at ambient temperature (A) and two pCO_2 treatments (380 and 750 ppm) at elevated temperature were simulated. These treatments are hereafter referred to as 380A, 750A and 1000A, and 380T and 750T, respectively. Ambient temperature was controlled to follow the seasonal cycle at the population source conditions (typically between 9 and 15 °C) and warming was simulated as a 2 °C offset above that variation (Queirós *et al.* 2015). Throughout the experiment, egg capsules laid by adults in the treatment tanks were inspected on a weekly basis, and hatched juveniles varying between one and 14 weeks of age were recorded and collected for later analyses. Out of this collection, only those of three and nine weeks of age were examined in the present study. The number of eggs and juveniles produced by the adults varied greatly between treatments, and in the 1000A treatment, only four individuals hatched in 14 months, possibly as the result of metabolic depression observed in adult *N. lapillus* (Queirós *et al.* 2015). Due to the low replication level, this treatment group was therefore excluded from the current analysis. Twenty-four individuals from the other four (OA x OW) treatments were collected at random and analysed, three from each age group and

148 treatment combination. All specimens were stored dry or in minimal amounts of distilled water at
149 -80 °C before, in between and after analyses, and transported in liquid nitrogen where necessary.
150
151
152 **Micro-CT scanning**
153 Scanning was carried out at the Hellenic Centre of Marine Research (Crete, Greece). Each
154 individual was inserted into an individual pipette tip which was sealed airtight and positioned
155 upright in the scan chamber of a micro-tomograph (Skyscan 1172, Bruker, Belgium). The scan
156 medium was always air, and no stains were used. Specimens were scanned with a voltage of 59
157 kV and a 167 µA current for the acquisition of morphological and density related data. Density
158 measurement calibration was achieved experimentally and from past measurements of similar
159 materials. The micro-tomograph has a maximum resolution of 4000 x 2672 pixels (~0.8 µm *per*
160 pixel). A filter with two layers of aluminium foil was used to minimise excess charge. These
161 settings were optimised for the highest resolution (4,000x), an exposure time of 1915 ms and
162 between 0.85 and 1.3 µm zoom, depending on the size of the specimen. Images were collected at
163 full 360° rotation with no random movement, and averaging every two images at every rotation
164 angle. Scanning parameters were recalibrated before each scan to ensure comparability between
165 image sets (*i.e*. individuals).
166
167 **Reconstruction of scanned specimens**
168 The micro-CT projections were reconstructed into cross-sectional images of shells using a
169 reconstruction software (NRecon, Skyscan, Bruker, Belgium), which is based on a modified
170 Feldkamp's back-projection algorithm (Feldkamp *et al.* 1984). This was accomplished as an
171 automated function of the scanning process using graphics processor unit reconstruction (GPU
172 recon). If specimens had inadvertently moved during image acquisition, the scan was repeated.
173 Reconstructed scans of tilted specimens were straightened to achieve a uniform measure of

length and width in 3D view (Dataviewer, Skyscan, Bruker, Belgium). Ten cross-sections of each shell (hereafter "slices") were reconstructed in pre-selected locations across the shell, which were standardised across individuals to optimise comparability between individual results (Fig. 1).

Scan analysis and data extraction

Shell length, width and thickness measurements were acquired using Dataviewer (Bruker 2014). Shell thickness was averaged across the widest part of the shell (WP1) as well as the Mid-lip slice (ML1; Figure 1). A 15 pixel thick band was selected from the edge of the shell and inwards around the outside of each of the ten slices for density measurements, using the software Image J1.45S (National Institutes of Health, USA). This band ensured that the selected area had been in immediate contact with the external conditions and not protected by soft tissue or body fluids. Shell density was measured as the average 2D grey-scale pixel intensity using the whole band.

The visual comparison of shell surface damage between individuals was accomplished in a volume rendering software (CTVox, Skyscan, Bruker, Belgium), where a 3D visualisation of the shells as image stacks was produced, manipulating factors such as opacity and lighting (Fig.2).

3D Geometric Morphometrics measurements

3D geometric morphometric methods were applied to the reconstructed 3D scans (i.e. shell plastic model, see Fig. 2) to investigate potential changes in shell morphology associated with phenotypic plasticity responses. Due to limits on computer memory during processing, scan file size was reduced and, consequently, resolution also reduced by a factor of 16. This was achieved using the Dataviewer resizing option prior to reconstructing triangulated surfaces for each of the specimens using the software Amira (FEI, 2013). Surfaces were reconstructed using the 'SurfaceGen' option on the resampled dataset and the resulting models were saved in 'Polygon File Format' (.ply). Overall, the scans were reduced in size by a factor of ~64, but only a low level of detail was lost post processing.

Surface models were then uploaded into software designed for the analysis and interpretation of three-dimensional shapes (Landmark editor, Wiley 2007). Here, a series of type 1 and 2 landmarks were introduced in the form of single landmarks and curves (Fig. 2) on the lip, on minimum and maximum points as well as on each end of and along the whorl.

By establishing this landmark protocol (Fig. 2) in the first shell and reproducing it in the others through correspondence of each set of landmarks with those of the original specimen, comparable measures of shape could be applied to the distinct features shared by all shells. Data points were exported from Landmark into MorphoJ (Klingenberg 2011) where models were adjusted in a procrustes fit: a forced adjustment of all involved models for the sake of comparability, before generating covariance matrices and conducting procrustes analyses. These measures were taken in order to achieve optimal shape alignment through scaling, rotation and translation of the models. Amira (FEI 2013), the programme used to make the original 3D models, was also used to measure the volume of each of the specimen's shells.

Analysis of crystalline properties

At Plymouth University (Plymouth, UK), scanned specimens were positioned on the bottom of cylindrical moulds with the youngest shell part facing downwards and fixed in this position on a thin layer of generic superglue. The mould was filled with epoxy resin and left in a vacuum chamber to de-gas, until the shells were enclosed inside and outside by the resin. The encased specimens were left at 30 °C over night to allow the epoxy resin to harden before sanding and polishing the formerly lower surface off to the desired cross-section.

Hand polishing was carried out using first abrasive paper (P800 and P2500, FEPA P-grade), then 1 µm fine diamond paste on a bench-top sander (Kemet Int. Ltd., UK) with a fabric disc as foundation for the paste. Cross-sections were taken from comparable points in all shells. The surface of each cross-section was further etched with hydrochloric acid for 45 s to improve the exposure of a shell surface for visualisation. Specimens were then carbon coated in a carbon

sputter-coater (K450X, EmiTech, Quorum Technologies, UK) using carbon rods. Scanning electron microscopic energy dispersive x-ray analysis (JEOL JSM-6610 LV, JEOL, Tokyo, Japan) was used to determine the crystalline structure of each shell, and the relative thickness of homogenous and crossed-lamellar layers were recorded, as possible. Where more than one crystal layer was present, x-ray spectra were selected from each of the cross-sections in the outermost layer of crystals to examine the most exposed regions. Images of each cross-section were taken for further analysis at appropriate magnification to determine crystal polymorph structure (Marxen *et al*. 2008). The elemental ratio from each x-ray spectrum was recorded (for technique see Reed 2005).

Statistical analysis

Shell weight, length, width, thickness, volume and density data sets were analysed separately and differences between treatment and age groups investigated. All data were screened on whether they met the assumptions of a linear model by assessing independence of errors, homoscedasticity and normality of residuals. Where assumptions were met, Analysis of Variance (ANOVA; Fisher 1925) was carried out for each response variable. Else, datasets we analysed using Generalized Least Squares (GLS; Cascetta 1984) modelling, wherein the best fitting and most parsimonious models were selected, based on Akaike's Information Criterion (AIC; Akaike 1973). The combined effects of temperature, pH and age on the similarity structures of the aggregated datasets (all response variables) were also investigated using crossed Analysis of Similarity (ANOSIM; Clarke 1993) and the software Primer (Clarke & Gorley 2014). This further step was undertaken to investigate whole-individual responses between treatments, allowing for consideration to be given to the potential variability in specific responses of individuals within treatment groups.

Additionally, similarity percentage tests (SIMPER; Clarke 1993) were used to determine which variables most explained observed variation in the chemical make-up of the shells (i.e. elemental

composition) between treatment and age groups. Statistical difference in chemical make-up of shells was tested between individuals as well as treatment- and age groups. Mean weights of each element within individual samples were then compared in Primer and R using crossed ANOSIM tests and GLS modelling. Out of all the elements (and element ratios) recorded in the spectral analysis, a special focus was put on analysing the magnesium:calcium ratios (Mg:Ca) because it is one of the factors determining crystallisation within the shells. Non-metric Multi-Dimensional scaling (nMDS; Kruskal 1964) was estimated based on Euclidean distances to explore overall dissimilarities between age and treatment groups. Unless otherwise specified, all data analyses were carried out in R (R foundation, Vienna).

Results

Shell surface

Shells of individuals exposed to elevated pCO_2 (i.e. 750 ppm, Fig. 3) exhibited overall a greater proportion of rough textures and indentures on their surface than at ambient pCO_2, in both age groups, and this effect that was more pronounced under co-occuring elevated temperature conditions (750T cf. 380A). This can also be seen in the cross-sectional images in figure 1, in which the shell exposed to high temperature and elevated pCO_2 (750T, Fig. 1C) showed a distinctly more uneven surface than the control shell (380A, Fig. 1B).

Shell micro-structure and chemistry

Shells' microstructures from individuals kept under control conditions (380A) exhibited a structure of separation into a neatly sorted crossed-lamellar (CL) inner layer of thin aragonitic $CaCO_3$ sheets and a thin, grainy homogenous (H) outer layer (Fig. 4, 380A, 1-3). Shells of individuals kept under the elevated temperature condition (380T) exhibited similar structures but the thickness of the layers varied. Crossed-lamellar crystals varied in size and neatness of layering and the H layers were smoother than in the control treatment group (Fig. 4, 380T, 1-3 cf. Fig.4, 380T). Shells kept at ambient temperature and elevated pCO_2 had lost the distinct layering and although both CL and H structures were recognisable, the transitional phase contained both (Fig. 4, 750A, 1). The biggest change in shell microstructure however was found in 9 weeks old individuals exposed to high pCO_2 at ambient temperature and in shells of all ages where both temperature and pCO_2 had been increased. Here, the newest shell parts (closest to the growth edge at the lip) displayed a complete lack of layering with a new crystal structure that resembled neither CL nor H patterns found in other shells (Fig. 4, 750T, 1-3). Although being most easily comparable to homogenous patterns, these new structures had eroded bark-like surfaces and little to no common direction of orientation of the crystals (Fig. 4, 750T, 3). Some of the older parts of shells from elevated temperature and pCO_2 conditions displayed an unusually thin CL layer. The CL structures in those

286 shells exhibited equally chaotically oriented crystals to what had been observed in 750A shells in
287 both layers, and H structures more closely resembling the bark-like new structure than what had
288 been recorded as H in 380A (Fig. 4, 750T, 1). Crystal degeneration and deformation was stronger
289 in the outermost parts of the shell than those closer to the columella.

290 The internal Mg:Ca ratio of the shells varied among individuals of different ages and exposures to
291 different temperatures ($p < 0.05$, Fig. 5, A). Testing the other elements found within shells with
292 SIMPER analyses confirmed variations in Ca^{2+} to be the greatest cause of dissimilarity between
293 most sample groups, especially between pCO_2 treatments (65.7 %) and age groups (65.1 %).
294 Variations between temperature groups were found to be due in equal parts to variation in
295 oxygen, carbon, calcium and magnesium proportions. The remaining deviations between age and
296 CO_2 groups can be explained through variations in oxygen content, though all samples also
297 contained traces of carbon and sodium.

298 **Shell density**

299 Shell density was found to be significantly lower in all experimental treatments when compared
300 to individuals kept under control conditions. Exceptions to this pattern were 9 weeks old snails
301 maintained at elevated temperature and pCO_2 treatment, which had the densest shells (750T).
302 Exposure to elevated pCO_2 alone decreased shell density, but only in the 9 week old juveniles. The
303 effects of age and temperature on shell density in isolation were less clear. The best GLS model
304 included as main effects and interactions temperature, age and CO_2-content (appendix 1, table 1,
305 $p< 0.01$, Fig.5, B).

306 **Shell growth and shape**

307 Groups of similar age and pCO_2 exhibited more variation shell morphology (*i.e*. length and shape)
308 at ambient than at warm conditions, suggesting that temperature increased shell variability. The
309 best GLS model for shell length included temperature, pCO_2 and age as main effects and

310 interaction ($p < 0.01$, appendix 1, table 2), suggesting that the effects of CO_2 and temperature on
311 the shell lengths of *N. lapillus* differed with age (Fig. 6, A).

312 With regard to shell width, young shells of similar temperature groups treated at elevated pCO_2
313 levels (750A and 750T) were narrower than those treated in control pCO_2 conditions (380A and
314 380T), yet the opposite was true for old shells, which were wider at higher CO_2 (Figure 6, B).
315 Indeed, this effect was clear from the GLS analysis of shell width, for which the best GLS model
316 included age and CO_2 as main effects and interaction, but not temperature ($p \leq 0.05$, appendix 1,
317 table 3).

318 **Shell thickness**

319 Similar to the patterns observed in other measurements, shells of young individuals exposed to
320 similar temperature treatments were distinctly thinner when exposed to higher CO_2
321 concentrations, while older shells were thicker in high CO_2 (Fig. 6, C). The best GLS model included
322 temperature, age and CO_2 as main effects and interaction ($p < 0.05$, appendix 1, table 4). Although
323 temperature appeared to have an effect on shell thickness, this effect was variable across age and
324 CO_2, and the effects of CO_2 and shell age were greater.

325

326 **3D geometric morphometric shape analysis**

327 As expected from the previous analyses, individuals variation in shell shape did not appear to be
328 determined by any factor investigated in isolation, but was instead was explained by the
329 combination of factors investigated, as represented by in the principle components ("PC") biplot
330 (Fig.7). PC1-3 represented the majority of the variance in both the younger (73.17 %, Fig. 7B) and
331 the older shells (77.22 %, Fig. 7A), representing mainly the angle and width of the shell whorl,
332 aperture shape and length and the overall length, together creating the difference between
333 narrower or wider shells. Whilst only a loose separation of the 750T individuals and those in the

380T treatment was apparent in the younger age group, PC2 (representing the shape of the whorl) clearly separated 750 ppm treatments (750A and 750T, positive PC score) from the 380 ppm treatments (380A and 380T, negative PC score) in the older age group. The latter likely reflects higher procrustes distances estimated for older shells, indicating that shell shape (as determined using landmark analysis) varied more in these the older than in the younger age group.

These results were confirmed by a two-way crossed ANOSIM analysis of externally measured data sets combined (length, width, density and thickness), which revealed that age (ANOSIM, global $R = 0.217$, $p < 0.05$) and CO_2 content (ANOSIM, global $R = 0.208$, $p < 0.05$) were the overall most deciding factors causing dissimilarities in shell variables. Differences in temperature, and the interaction of temperature with other factors however were not. All variables (lengths, width, density and thickness) contributed roughly equal amounts of variation to the dissimilarities between groups (~20% each). Three-week old individuals were more similar to each other in shape (Figure 8), roughly clustering in the middle of the nMDS plot. Nine-week old individuals were distributed more widely around the edges of the plot, exhibiting greater variability in shape and in the relations between the different shape variables, and highlighting the role of treatments on shell development as time passed. The control group (380A) had the least within-group variation when compared with the others, with animals clustering in the centre of the nMDS plot, while the most extreme 750T treatment led to greater dissimilarity in external shell characteristics

Discussion

While the majority of structural shell features in juveniles of the gastropod *N. lapillus* appear to be influenced significantly by elevated pCO_2 and a two degree temperature offset on the temperature seasonal cycle, the impacts of these effects change as juveniles develop. Overall, the effects of CO_2 elevation and differences between age groups were evident, while higher temperatures appeared to act as a modifier of juveniles' responses to pCO_2. Differences in response between age groups may reflect how younger individuals are likely less capable to maintain their homeostasis and compensate for the increase in energy expenditure needed to upkeep shell structures. The differences observed between age groups may also likely reflect potential differences in parental investments in reproduction, given that the adults' metabolism and energy requirements were found to be significantly affected by exposure to both elevated pCO_2 and temperature during the 14-month mesocosm experiment (Queirós *et al*. 2015). *N. lapillus* typically show a great deal of shell phenotypic plasticity when exposed to OA and OW conditions and our findings are in line with previous work showing shells' plastic responses to be more marked in individuals exposed to elevated temperature and pCO_2 conditions (Lardies *et al.* 2014). This may be a consequence of individuals' physiological trade-offs (Turner *et al.* 2015), here specifically between shell formation and repair *versus* maintaining cellular metabolism and homeostasis. These findings are particularly relevant for *N. lapillus* ecology, because external shells provide a first barrier against predation, physiological and mechanical stress. Compensatory processes involved in shell deposition in *N. lapillus* may therefore prove beneficial under near future ocean conditions.

A significant reduction of shell growth and thickness after exposure to elevated pCO_2 has also been observed in other species (Barros *et al.* 2013, Sanford *et al.* 2014) and is thought to be linked to associated alteration of carbonate chemistry and growth inhibition in molluscs. Both of these effects make the organisms more vulnerable to crushing predators, such as crabs (Hughes & Elner 1979) and might therefore lead to increased mortality rates in affected populations. It is unclear

380 whether *N. lapillus* growth rates are affected by the higher CO_2 content directly, yet this study
381 indicates that shell development was certainly modified. Importantly, and in contrast to previous
382 studies, we found that as *N. lapillus* grew, older juveniles exhibited potentially compensatory
383 responses. In older juveniles, shells were wider, longer and thicker under elevated pCO_2,
384 potentially serving as a better defence. Despite evidence for increased surface damage and
385 dissolution, potentially higher calcification rates may therefore in part have compensated for
386 greater passive dissolution rates. This finding agrees with Melatunan *et al.* (2013) who, while
387 focusing on adult gastropods, also found advantageous adaptations that allowed shell shape and
388 size changes in molluscs affected by an offset in CO_2 content. Whether increased shell size is seen
389 as adaptively advantageous overall is, however, not clear, because larger shells may attract
390 greater risk of crab predation (Cotton *et al*. 2004).

391 In general, gastropod shells are strengthened gradually through continuous calcification from
392 within, leading to the thickening of the existing shell walls with age, as well as the establishing of a
393 stronger microstructure in older shells (Weiss *et al*. 2002). Mg:Ca ratios of calcifiers track the ratio
394 of these minerals in seawater (Ries *et al*. 2010) . Concordantly, higher Mg:Ca ratios observed here
395 in the shells of individuals exposed to elevated pCO_2 suggest that this elemental ratio increased in
396 in those treatments. Higher Mg:Ca ratio in seawater is indeed known to favour the formation of
397 Mg rich aragonite, instead of calcite (Ries *et al*. 2010, Smith *et al*. 2006), though seawater was not
398 undersaturated for calcite or aragonite during our experiments (Queirós *et al*. 2015,
399 Supplementary Information Table SI). *N. lapillus* may therefore have a delayed transition from
400 aragonite to calcite in more energetically challenging conditions (such as OA) as the former is less
401 energetically demanding to deposit, particularly under in low pH scenarios (Weiss *et al.* 2002).
402 This mechanism could explain the wider, longer and thicker shells observed in the older juveniles
403 from the high pCO_2 treatments in relation to the control, as though through this delay, more
404 energy may have been available for the potentially increased calcification rate needed to address
405 the greater shell damages observed in this treatment. Therefore, *N. lapillus* may have the ability

406 to compensate, at least at this early stage of development, against the potential negative effects
407 of carbonate chemistry conditions imposed by high CO_2 on shell deposition and dissolution. In line
408 with recent findings (Fitzer *et al.* 2016), the microstructure of the material deposited though this
409 compensation exhibited a more chaotic $CaCO_3$ crystal formation. $CaCO_3$ microstructure strongly
410 depends upon the presence of specific types of proteins in the extrapallial fluids (Bozhi 2011). As
411 these proteins are influenced by pH conditions (Thomsen *et al.*, 2010; Thompson *et al.* 2000),
412 organisms have been observed to alter crystallisation patterns in high CO_2 conditions (Cusack *et*
413 *al.* 2007). The main shell building protein in *N. lapillus* is dermatopontin, which is 'acid soluble'
414 (Suzuki & Nagasawa 2013). Based on our results it is likely that even though these proteins are
415 isolated from surrounding conditions, lower pH in the paleal fluid may have been present in
416 individuals exposed to higher CO_2 contents, affecting the quality of crystallisation within the shell.
417 In some cases, proteins sensitive to low pH conditions can be substituted through the production
418 of a range of different, less pH susceptible proteins (Hüning *et al.* 2012), but this does not seem to
419 be the case here.

420 The most important functions of complex shell structures are to provide structural support and
421 protection from predator and physical stresses (e.g. wave action), which may cause the shell to
422 crack or even break. The crossed-lamellar structures commonly found in the shell of healthy *N.*
423 *lapillus* individuals prevent cracks in the shell from propagating through a constant change in
424 crystal orientation (Suzuki & Nagasawa, 2013). Therefore, a thicker shell does not necessarily
425 provide a better protection against predation if the cross-lamellar structure has disappeared, as
426 we observed in the shells of juvenile snails exposed to elevated pCO_2, which were exacerbated by
427 an elevation in temperature. Bark-like crystal shapes such as the ones found in the acidified
428 samples in this study seem to be a phenomenon not yet widely described in the literature. Seeing
429 as the current literature is still dominated by short-term single stressors studies of adult
430 specimens, our results highlight the need to investigate the development of shell mineralogy and
431 ultrastructure in juvenile molluscs under high temperature and CO_2 environments, over extended

time periods, and considering the cumulative effects of exposure (such as here and in Dupont *et al*. 2013). Adult individuals transplanted into conditions of elevated pCO_2 exhibit distinctly different calcification patterns in localised, newly built shell areas, including unorganised crystals with varying growth directions (Hahn *et al*., 2011). However, the impact of high CO_2 content (and high temperatures) on shell physiology, as observed here, may still lead juveniles to higher vulnerability to predation and physical damage, despite the potential for adaptive processes taking place during shell deposition. Crystallisation processes are similar in many organisms, even in far related groups, such as brachiopods, suggesting that the results from this study may be generalised to the impacts of similar conditions on the shell formation of juveniles of other species (Cusack *et al.* 2007).

Shell volume and weight were not impacted by exposure to elevated pCO_2 or temperature nor by the combination of the two factors, and surprisingly neither differed significantly among snails of different age classes in our experiment. Insignificant differences in shell volume may be due to the differences in shell shape we observed across treatments. A shape change may lead to shells that are more stout or narrow, consequentially changing shell size but not volume. Thicker shells in acidified treatments were also less dense (as seen in adult *N. lapillus*, Queirós *et al.* 2015), possibly explaining the lack of significant changes in shell weight. In our experiment, differences in shell shape were also not consistent across age groups, indicating that as *Nucella* grow, some compensatory responses seem to take place that affect its shape. Younger shells of both control pCO_2 treatments were most antithetic to one another while in the older groups it were shells from ambient pCO_2 combined with elevated temperature, as well as shells from elevated temperature combined with ambient temperature treatments. Gastropod morphology varies with environmental pressures such as predation, wave action and desiccation, substrate, $CaCO_3$ and O_2 concentration and temperature (Langerhans & Dewitt 2002, Hollander *et al*. 2006, Queiroga *et al*. 2011). Although water chemistry, pH and temperature have also been known to affect molluscs' shell shapes (Melatunan *et al*. 2013), the main factors influencing gastropods seem to be more of

458 a more mechanical nature, namely predation and wave pressure (Queiroga *et al*. 2011,
459 Langerhans & Dewitt 2002). Shell slandering and squatting as seen in Guerra-Varela *et al*. (2009)
460 prevents shells from being swept away by waves as well as making it harder for predators to crush
461 them. The findings we observed here regarding shell shape further suggest that high CO_2 contents
462 will potentially make young *N. lapillus* more vulnerable to both pressures, as shells became longer
463 and stouter. Shells that are structurally weakened in this way are more likely to become easy prey
464 to shell-crushing predators such as crabs (*e.g.* Melatunan *et al.* 2013). The shell variability we
465 observed within treatment groups may be partly due to the fact that the embryonic development
466 takes place within individual egg capsules which can lead to variations in size and developmental
467 rate (Thorson, 1950). Differences in parental investment may also be a deciding factor of
468 variability within age groups (Órdenes & Antonio 2012). In this study, the duration of elevated
469 pCO_2 and temperature exposure of the adults at the time of reproduction has not been taken into
470 account because we could trace parental links within the experimental replicate, but this could
471 have driven some of variation we observed within treatment groups that was not assignable to
472 specific the treatments. This is a factor that should be considered in future studies.

473 The impact of elevated pCO_2 and temperature treatments on shell properties and growth pattern
474 may lead to important implications for the size, shape and structural integrity of shells in adult *N.*
475 *lapillus* in a future ocean. We observed very little reproductive output in *N. lapillus* from our
476 highest CO_2 treatment, though a congeneric *Nucella* species occurs and grows in natural vents
477 (Selin 2010), and as *Nucella* are direct developers, reliance on lateral input of individuals from
478 adjacent areas seems unlikely. Survival and viable reproduction of *N. lapillus* therefore seems
479 possible below or even up to 1000 ppm of CO_2, though the viability of offspring may be limited at
480 this high level of pCO_2 (Queirós *et al*. 2015). At this most extreme pCO_2 level, expected in about a
481 century according to projections reviewed by the IPPC (2014) in which seawater CO_2 may reach
482 1000 ppm, the combination of decreased investment in offspring by adults (4 juveniles born in 14
483 months, compared to 280 that were born in control conditions in the same time) and the

484 observed impairment of the protective shell structures of juveniles leading to increased juvenile
485 mortalities paint a bleak picture for *Nucella* in the near future ocean. Queirós *et al.* (2015) found
486 that sea warming may counter-act metabolic depression caused by elevated pCO_2 in adult *N.*
487 *lapillus*, and that decrease in prey acquisition due to limited chemo-sensory function under high
488 CO_2 may be counter-acted by adaptive predatory behaviour, in the absence of predators.
489 However, weakened shell structures that make *N. lapillus* more vulnerable to predation may
490 hinder the latter, both in adults and juveniles, as the observed altered predation behaviour
491 requires more extensive foraging times and would therefore expose the individuals to predators
492 for longer periods of time. It follows that, overall, *Nucella lapillus* and other calcifiers with similar
493 ecology are more likely to suffer from the effects of climate change and acidification than to
494 benefit from it. *N. lapillus*'s predation on important habitat forming species plays a key role in the
495 shaping the biodiversity of temperate rocky shores and so these findings have potentially
496 important consequences for the structuring of these communities under near future ocean
497 conditions.

498 **Conclusion**

499 Queirós *et al*. (2015) found that, considering a large number of ecological processes, *N. lapillus*
500 populations from highly productive areas may be more likely to be able to compensate for the
501 energetically costly effects of elevated pCO_2 and temperature levels. Nevertheless, changes to the
502 shell development, morphology and composition of juvenile *N. lapillus* exposed to high pCO_2 and
503 temperature conditions observed in this study may lead to higher predation risks. Thus, though
504 some populations may be expected to be more heavily affected by OA and OW than others,
505 considering the low dispersal rates of *Nucella* due to the direct development, changes in
506 distributional ranges may be foreseen through this enhanced sensitivity of the juvenile stage.
507 Sustainability of populations in regions changing less within the near future and in populations
508 with exceptionally wide genome range could be expected, as some phenotypic plasticity was
509 observed, even within our across-generation study (Lardies *et al*. 2014, Sunday *et al*. 2014).

510 However, even sub-lethal effects can affect communities in composition and fitness (Parker *et al*.
511 2013), and sub-lethal modifications that may be seen as adaptive, e.g. in behaviour, may be
512 detrimental within a community setting (Queirós *et al.* 2015). This study highlights that changes in
513 CO_2 content and temperature may impact natural populations *via* effects on early-life stages and
514 developmental plasticity that are not evident in adults, and a large gap remains about how
515 population-level effects of OA and OW may scale to natural systems, in the context of whole
516 communities.

517

518 **Acknowledgements**

519 This study was undertaken as part of a Master's thesis, as an added-value activity within NERC-
520 DEFRA-DECC funded UK Ocean Acidification Research Programme (grant agreement
521 NE/H01747X/1). Analyses of impacts on shell structure were supported by the Research
522 Programme AcidiCO_2ceans funded by the Latsis Foundation (Greece). SR was awarded a
523 Santander Internationalization Postgraduate Scholarship that supported this work. PC is
524 supported by a NSERC Discovery Grant. Joana Nunes, and other staff and students at Plymouth
525 Marine Laboratory are thanked for support provided during the mesocosm experiments at PML.
526 Nafsika Papageorgiou (HCMR) is thanked for her kind support and advice during the stay of SR at
527 HCMR. Glenn Harper, Peter Bond, Terry Richards, and Roy Moate at Plymouth University are
528 thanked for aiding with the development of the methodology for specimens preparation and
529 subsequent electron microscopic imaging and x-ray spectra acquisition. Andrew Foggo is thanked
530 for support in travel through Plymouth University.

531

532

533 **References**

534 Akaike, H. 1973. Information theory and an extension of the maximum likelihood principle. In 2nd
535 International Symposium on Information Theory, Tsahkadsor, Armenia, USSR, September 2-8,
536 1971. Ed. by Petrov, B.N. and Csáki, F. Akadémiai Kiadó, Budapest. 267-281.

537 Barros, P., Sobral, P., Range, P., Chicharo, L., Matias, D. 2013. Effects of sea-water acidification on
538 fertilization and larval development of the oyster *Crassostrea gigas*, Journal of Experimental
539 Marine Biology and Ecology, 440, 200-206

540 Bozhi, J. 2011. Screening of molluscan extrapallial proteins on $CaCO_3$ crystallisation via
541 microfluidics. PhD thesis, University of Glasgow

542 Bruker 2014. *DATAVIEWER v1.5.1*. Bruker microCT. Kontich, Belgium

543 Brusca, R.C., Brusca, G.J. 2003. *Invertebrates*. Sinauer Associates, 2nd Edition

544 Byrne, M., Przesllawski, R. 2013. Multistressor impacts of warming and acidification of the ocean
545 on marine invertebrates' life histories. Integrative and Comparative Biology. 53: 1-15

546 Calosi, P., Rastrick, S. P., Lombardi, C., de Guzman, H. J., Davidson, L., Jahnke, M., *et al*. 2013.
547 Adaptation and acclimatization to ocean acidification in marine ectotherms: an in situ transplant
548 experiment with polychaetes at a shallow CO_2 vent system. Philosophical Transactions of the
549 Royal Society of London B: Biological Sciences. 368: 1627

550 Cascetta, E. 1984. Estimation of trip matrices from traffic counts and survey data: A Generalized
551 Least Squares estimator, Transportation Research. 18: 289-299

552 Clarke, K. R. 1993. Non-parametric multivariate analyses of changes in community structure.
553 Australian Journal of Ecology. 18: 117-143

554 Clarke, B., Gorley, R. 2014. Primer 6. PRIMER-E Ltd., Ivybridge, UK

555 Cotton, P.A., Rundle, S.D., Smith, K.E. 2004. Trait compensation in marine Gastropods: Shell
556 shape, avoidance behavior, and susceptibility to predation. Ecology. 85: 1581-1584

557 Cusack, M., Perez-Huerta, A., Dalbeck, P. 2007. Common crystallographic control in calcite
558 biomineralisation of bivalve shells. CrystEngComm. 9: 1215-1218

559 Dupont, S., Thorndyke,M. C. 2009. Impact of CO_2-driven ocean acidification on invertebrates early
560 life-history – What we know, what we need to know and what we can do. Biogeosciences
561 Discussions. 6: 3109-3131

562 Dupont, S., Dorey, N., Stumpp, M., Melzner, F., & Thorndyke, M. 2013. Long-term and trans-life-
563 cycle effects of exposure to ocean acidification in the green sea urchin *Strongylocentrotus*
564 *droebachiensis*. Marine Biology. 160: 1835-1843

565 Falini, S., Albeck, S., Weiner, S., Addadi, L. 1996. Control of aragonite polymorphism by mollusk
566 shell macromolecules. Science. 271: 67-69

567 Feely, R.A., Sabine, C.L., Lee, K., Berelson, W., Kleypas, J., Fabry, V.J., Millero, F.J. 2004. Impact of
568 anthropogenic CO_2 on the $CaCo_3$ systems in the oceans. Science. 305: 362-366

569 FEI 2013. *Amira 5.5*, Visualization Sciences Group. FEI Company. Burlington, USA

570 Feldkamp, L., Davis, L., Kress, J. 1984. Practical cone-beam algorithm. Journal of the Optical
571 Society of America, 1: 612-619

572 Findlay, H.S., Kendall, M.A., Spicer, J.I., Widdicombe, S. 2010. Post-larval development of two
573 intertidal barnacles at elevated CO_2 and temperature. Marine Biology. 157: 725-735

574 Findlay, H.S., Beesley, A., Dashfield, S., Mcneill, C.L., Nunes, J., Queirós, A.M., Woodward, E.M.S.
575 2013. UKOA Benthic Consortium, PML intertidal mesocosm experimental environment dataset (ed
576 Laboratory PM). British Oceanographic Data Centre - Natural Environment Research Council, UK

577 Fisher, R. A. 1925. Statistical methods for research workers. Genesis Publishing Pvt Ltd.

578 Fitzer, S. C., Chung, P., Maccherozzi, F., Dhesi, S. S., Kamenos, N. A., Phoenix, V. R., & Cusack, M.
579 2016. Biomineral shell formation under ocean acidification: a shift from order to chaos. Scientific
580 reports, *6*.

581 Green, M.A., Jones, M.E., Boudreau, C.L., Moore, R.L., Westman, B.A. 2004. Dissolution mortality
582 of juvenile bivalves in coastal marine deposits. Journal ofLimnology and Oceanography. 49: 727-
583 734

584 Guerra-Varela, J., Colson, I., Backeljau, T., Breugelmans, K., Hughes, R. N., & Rolán-Alvarez, E.
585 2009. The evolutionary mechanism maintaining shell shape and molecular differentiation
586 between two ecotypes of the dogwhelk *Nucella lapillus*. Evolutionary Ecology. *23*: 261-280

587 Hahn, S., Rodolfo-Metalpa, R., Griesshaber, E., Schmahl, W.W., Buhl, D., Hall-Spencer, J.M.,
588 Baggini, C., Fehr, K.T., Immenhauser, A. 2011. Marine bivalve geochemistry and shell
589 ultrastructures from modern low pH environments. Biogeosciences Discussions. 8: 10351-10388

590 Hollander, J., Collyer, M.L., Adams, D.C., Johannesson, K. 2006. Phenotypic plasticity in two
591 marine snails: constraints superseding life history. The Authors Journal Compilation. 19: 1861-
592 1872

593 Hughes, R.N., Elner, R. 1979. Tactics of a predator, *Carcinus maenas*, and morphological responses
594 of the prey, *Nucella lapillus*. The Journal of Animal Ecology. 48: 65-78

595 Hüning, A.K., Melzner, F., Thomsen, J., Gutowska, M.A., Krämer, L., Frickenhaus, S. *et al.* 2012.
596 Impacts of seawater acidification on mantle gene expression patterns of the Baltic Sea blue
597 mussel: implications for shell formation and energy metabolism. Marine Biology. 160: 1-17

598 IPPC 2014. Summary for Policymakers, In: Climate Change 2014: The Physical Science Basis.
599 Cambridge University Press, Cambridge, United Kingdom and New York, USA

600 Klingenberg, C.P. 2011. MorphoJ: an integrated software package for geometric morphometrics,
601 Molecular Ecology Resources. 11: 353-357

602 Kroeker, K.J., Kordas, R.L., Crim, R.N., Singh, G.G. 2010. Meta-analysis reveals negative yet variable
603 effects of ocean acidification on marine organisms. Ecology Letters. 13: 1419-1434

604 Kruskal, J.B. 1964. Multidimensional scaling by optimizing goodness of fit to a nonmetric
605 hypothesis. Psychometrika. 29: 1-27

606 Kurihara, H. 2008. Effects of CO_2-driven ocean acidification on the early developmental stages of
607 invertebrates. Marine Ecology Progress Series. 373: 275-284

608 Langerhans, R.B., Dewitt, T.J. 2002. Plasticity constrained: over-generalized induction cues cause
609 maladaptive phenotypes. Evolutionary Ecology Research. 4**:** 857-870

610 Lardies, M.A., Arias, M.B., Poupin, M.J., Manriquez, P.H., Torres, P.H., Vargas, C.A., Navarro, J.M.,
611 Lagos, N.A. 2014. Differential response to ocean acidification in physiological traits of *Concholepas*
612 *concholepas* populations. Journal of Sea Research. 90: 127-134

613 Marxen, J.C., Prymak, O., Beckmann, F., Neues, F., Epple, M. 2008. Embryonic shell formation in
614 the snail *Biomphalaria glabrata*: A comparison between scanning electron microscopy (SEM) and
615 synchrotron radiation microcomputer tomography (SRμCT). Journal of Molluscan Studies. 74: 19-
616 25

617 Melatunan, S., Calosi, P., Rundle, S.D., Widdicombe, S., Moody, A.J. 2013. Effects of ocean
618 acidification and elevated temperature in shell plasticity and its energetic basis in an intertidal
619 gastropod. Marine Ecology Progress Series. 472: 155-168

620 Melzner, F., Thomsen, J., Koeve, W., Oschlies, A., Gutowska, M.A., Bange, H.W., Hansen, H.P.,
621 Körzinger, A. 2013. Future ocean acidification will be amplified by hypoxia in coastal habitats.
622 Marine Biology. 160: 1875-1888

623 Nienhuis, S., Palmer, A.R., Harley, C.D.G. 2010. Elevated CO_2 affects shell dissolution rate but not
624 calcification rate in a marine snail. Proceedings of the Royal Society of Biological Sciences. 277:
625 2553-2558

626 Órdenes, C., Antonio, S. 2012. Offspring size, provisioning and performance as a function of
627 maternal investment in direct developing whelks. PhD Thesis, Victoria University of Wellington,
628 New Zealand

629 Parker, L.M., Ross, P.M., O'Connor, W.A., Pörtner, H.O., Scanes, E., Wright, J.M. 2013. Predicting
630 the Response of Molluscs to the Impact of Ocean Acidification. Biology. 2: 651-692

631 Plummer, L.N., Busenberg, E. 1982. The solubilities of calcite, aragonite and vaterite in CO_2-H_2O
632 solutions between 0-90 °C, and an evaluation of the aqueous model for the system $CaCO_3$-CO_2-
633 H_2O. Geochimica e Cosmochimica Acta. 46: 1011-1040

634 Queiroga, H., Costa, R., Leonardo, N., Soares, D., Clearly, D.F.R. 2011. Morphometric variation in
635 two intertidal littorinoid gastropods. Contributions to Zoology. 80: 201-211

636 Queirós, A. M., Fernandes, J. A., Faulwetter, S., Nunes, J., Rastrick, S. P. S, Mieszkowska, N., Artioli,
637 Y. *et al.* 2015. Scaling up experimental ocean acidification and warming research: from individuals
638 to the ecosystem, Global Change Biology. 21: 130-143

639 Reed, S.J.B. 2005. Electron Microprobe Analysis and Scanning Electron Microscopy in Geology.
640 Cambridge University Press. Cambridge, UK

641 Reusch, T. B. 2014. Climate change in the oceans: evolutionary versus phenotypically plastic
642 responses of marine animals and plants. Evolutionary Applications. *7*: 104-122.

643 Ries, J.B., Cohen, A.L., McCorkle, D.C. 2009. Marine calcifiers exhibit mixed responses to CO_2-
644 induced ocean acidification. Geology. 37: 1131-1134

645 Ries, J.B. 2010. Review: geological and experimental evidence for secular variation in seawater
646 Mg:Ca (calcite-aragonite seas) and its effects on marine biological calcification. Biogeosciences. 7**:**
647 2795-2849

Sanford, E., Gaylord, B., Hettinger, A., Lenz, E.A., Meyer, K., Hill, T.M. 2014. Ocean acidification increases the vulnerability of native oysters to predation by invasive snails. Proceedings of the Royal Society of Biological Sciences. 281: 1-8

Selin, N. 2010. Peculiarities of the habitat of Nucella freycineti (Mollusca: Gastropoda) at volcanogenic vent sites. Russian Journal of Marine Biology. 36: 26-33

Smith, A.M., Key Jr., M.M., Gordon, D.P. 2006. Skeletal mineralogy of bryozoans: Taxonomic and temporal patterns. Earth-Science Reviews. 78: 287-306

Sunday, J. M., Calosi, P., Dupont, S., Munday, P. L., Stillman, J. H., & Reusch, T. B. 2014. Evolution in an acidifying ocean. Trends in Ecology & Evolution. 29: 117-125

Suzuki, M, Nagasawa, H. 2013. Shell structures and their formation mechanisms. Canadian Journal of Zoology. 91: 349-366

Thompson, J.B., Palcoczi, G.T., Kindt, J.H., Michenfelder, M., Smith, B.L., Stucky, G., Morse, D.E., Hansma, P.K. 2000. Direct observation of the transition from calcite to aragonite growth as induced by abalone shell proteins. Biophysical Journal. 79: 3307-3312

Thomsen, J., Gutowska, M.A., Saphörster, J., Heinemann, A., Trübenbach, K., Fietzke, J., Hiebenthal, C., Eisenhauer, A., Körzinger, A., Wahl, M., Melzner, F. 2010. Calcifying invertebrates succeed in a naturally CO_2 enriched coastal habitat but are threatened by high levels of future acidification. Biosciences Discussions. 7: 5119-5156

Thorson, G. 1950. Reproductive and larval ecology of marine bottom invertebrates. Biology Revisions. 25: 1-45

Trussel. G.C., Ewanchuck, P.J., Bertness, M.D. 2003. Trait-mediated effects in rocky intertidal food chains: predator risk cues alter prey feeding rates. Ecology. 84: 629-640

Turner, L. M., Ricevuto, E., Massa-Gallucci, A., Gambi, M. C., & Calosi, P. 2015. Energy metabolism and cellular homeostasis trade-offs provide the basis for a new type of sensitivity to ocean acidification in a marine polychaete at a high-CO_2 vent: adenylate and phosphagen energy pools versus carbonic anhydrase. Journal of Experimental Biology. 218: 2148-2151

674 Vermeij, G.J. 1995. A natural history of shells. Princeton, NJ: Princeton University Press

675 Weiss, I.M., Tuross, N., Addadi, L., Weiner, S. 2002. Mollusc larval shell formation: Amorphous

676 calcium carbonate is a precursor phase for aragonite. Journal of Experimental Zoology. 293: 478-

677 491

678 Widdicombe, S., Spicer, J.I. 2008. Predicting the impact of ocean acidification on benthic

679 biodiversity: What can animal physiology tell us?. Journal of Experimental Marine Biology and

680 Ecology. 366: 187-197

681 Wiley, D.F. 2007. *Landmark 3.6*. Institute of Data Analysis and Visualization (IDAV). University of

682 California, Davis, USA

683 **Figures Legends:**

684 **Figure 1**

685 (A) Cross-sectional image of a nine week old *Nucella* shell taken with the micro-CT scanner,
686 indicating the position of the horizontal shell slices used for analysis. ELS = 3 % from the top
687 (posterior), AS1 = 3 % from the bottom (anterior), AS2 = 4 % from the bottom, AS3 = 5 % from the
688 bottom, WP1 = Widest Point, WP2 = WP1+1 %, WP3 = WP1-1 %, ML1 = Mid-Lip, ML2 = Mid-Lip
689 +1 %, ML3 = Mid-Lip -1 %. Lighter colour indicates higher shell density, while black illustrates the
690 background medium (air), not included in the analysis. 1 (B) and (C) are horizontal slices which
691 illustrate the differences in density throughout two randomly selected three week old shells. (B) is
692 a shell from ambient conditions (380ppm CO_2 / 9-15 °C), while (C) was exposed to elevated
693 temperatures and CO_2 input (750ppm CO_2 / 9-15 +2 °C) . Colours represent densities: green:
694 denser areas, blue: less dense areas. The scale bar below the vertically cross-sectioned shell
695 equates to roughly 0.5 mm.

696 **Figure 2**

697 Surface model of a shell, reconstructed using µ-CT. The landmark protocol used in this study to
698 evaluate shell morphology is represented by the red curves and dots. S0-S3 are single landmarks
699 while C1 and C2 represent curves.

700 **Figure 3**

701 Images of shell exteriors taken with the electron microscope (EM) to show examples of surface
702 damage in 750T (left) and 750A (right) shells.

703 **Figure 4**

704 Electron microscopy images of the crystallised structures within shells of the older group in lines
705 according to treatments; columns 1 represents a view of both layers together, 2 shows a close-up

706 of the crossed-lamellar layer, and column 3 are images of the homogenous structures. The first
707 picture depicting the 750T treatment represents a shell with no distinct difference between
708 layers, the second in that line shows an example of a shell with remnants of crossed-lamellar
709 structuring and the third picture is a close-up of the bark-like structure.

710 **Figure 5**

711 The effect of exposure to elevated pCO_2 and temperature, in juveniles of *N. lapillus* of different
712 age (weeks 3 and week 9 post exposure) on shell (A) Mg^{2+}:Ca^{2+} ratios and (B) density which are
713 coded along the x-axis with a combination of pCO_2 content (380 or 750 µatm), temperature (A for
714 ambient, T for elevated by 2 °C) and age (3 and 9 weeks). Where the graph displays a Mg:Ca ratio
715 of 0, this is due to 0 specimens having been available for this analysis from that treatment rather
716 than a ratio of 0.

717 **Figure 6**

718 The effects of exposure to elevated pCO_2 and temperature, in juveniles of *N. lapillus* of different
719 age (weeks 3 and 9 post exposure) on shell (A) length, (B) width and (C) thickness which are coded
720 along the x-axis with a combination of CO_2 content (380 or 750), temperature (A for ambient, T
721 for elevated) and age (3 and 9 weeks).

722 **Figure 7**

723 PC1 and PC2 of nine week old shells to the left (A) and three weeks old shells to the right (B)

724 **Figure 8**

725 nMDS plot of similarities and dissimilarities between individuals according to age and treatment
726 groups.

727

728

729

730

731 **Figures:** submitted in separate files (see tiff files labelled fig1-fig8)

732

733 **Tables:**

734

735 **Table 1: GLS test results concerning shell density:**

736 Significant results ($p < 0.05$) are bold.

737 Temp = temperature treatment, CO_2 = CO_2 treatment, Age = Age group

	AIC	BIC	likelihood	probability(χ²)
Temp*CO_2*Age	**146.79**	**156.62**	**-64.40**	**0.0024**
Temp*Age	**151.72**	**157.18**	**-70.86**	**0.026**
Temp*CO_2	**153.34**	**158.80**	**-71.67**	**0.054**
Age*CO_2	**151.72**	**157.18**	**-70.86**	**0.026**
Temp+Age+CO_2	156.09	161.54	-73.04	0.179
Temp+Age	157.50	161.86	-74.75	0.473
Age+CO_2	155.07	159.44	-73.54	0.141
Temp+CO_2	154.71	159.07	-73.35	0.117
Age	156.06	159.33	-75.03	0.334
CO_2	153.83	157.11	-73.91	0.075
Temp	156.32	159.60	-7.515.89	0.412

738

Table 2: GLS test results concerning shell length:

Significant results ($p < 0.05$) are bold.

Temp = temperature treatment, CO_2 = CO_2 treatment, Age = Age group

	AIC	BIC	likelihood	probability(p)
Temp*Age*CO_2	**5.91**	**15.73**	**6.046**	**0.0014**
Temp*Age	16.27	21.73	-3.14	0.159
Temp*CO_2	17.99	23.44	-3.99	0.326
Age*CO_2	**9.01**	**14.46**	**0.49**	**0.006**
Temp+Age+CO_2	16.83	22.28	-3.41	0.202
Temp+Age	15.51	19.88	-3.76	0.140
Age+CO_2	16.61	20.97	-4.30	0.242
Temp+CO_2	16.86	21.22	-4.43	0.273
Age	15.06	18.33	-4.53	0.122
CO_2	16.86	20.13	-5.43	0.441
Temp	15.72	18.99	-4.86	0.189

Table 3: GLS test results concerning shell width:

Significant results ($p < 0.05$) are bold.

Temp = temperature treatment, CO2 = CO_2 treatment, Age = Age group

	AIC	BIC	likelihood	probability(p)
Temp*Age*CO_2	-22.85	-13.031	20.43	0.082
Temp*Age	-19.37	-13.91	14.68	0.777
Temp*CO_2	-20.12	-14.67	15.06	0.602
Age*CO_2	**-25.91**	**-20.45**	**17.95**	**0.054**
Temp+Age+CO_2	-19.09	-13.63	14.54	0.844
Temp+Age	-21.08	-16.72	14.54	0.665
Age+CO_2	-20.35	-15.99	14.18	0.957
Temp+CO_2	-20.98	-16.62	14.49	0.699
Age	-22.33	-19.06	14.16	0.800
CO_2	-22.30	-19.02	14.145	0.860
Temp	-22.97	-19.70	14.48	0.401

739

Table 4: GLS test results concerning shell thickness:

Significant results ($p < 0.05$) are bold.

Temp = temperature treatment, CO2 = CO_2 treatment, Age = Age group

	AIC	BIC	likelihood	probability(p)
Temp*Age*CO_2	**-133.09**	**-123.27**	**75.54**	**0.035**
Temp*Age	-128.49	-123.04	69.25	0.475
Temp*CO_2	-126.67	-121.22	68.34	0.878
Age*CO_2	**-138.58**	**-133.13**	**74.29**	**0.005**
Temp+Age+CO_2	-128.31	-122.85	69.15	0.509
Temp+Age	-130.21	-125.84	69.10	0.331
Age+CO_2	-129.93	-125.57	68.96	0.379
Temp+CO_2	-128.65	-124.28	68.32	0.720
Age	-131.86	-128.59	68.93	0.171
CO_2	-130.13	-126.86	68.06	0.712
Temp	-130.46	-127.18	68.23	0.495

740

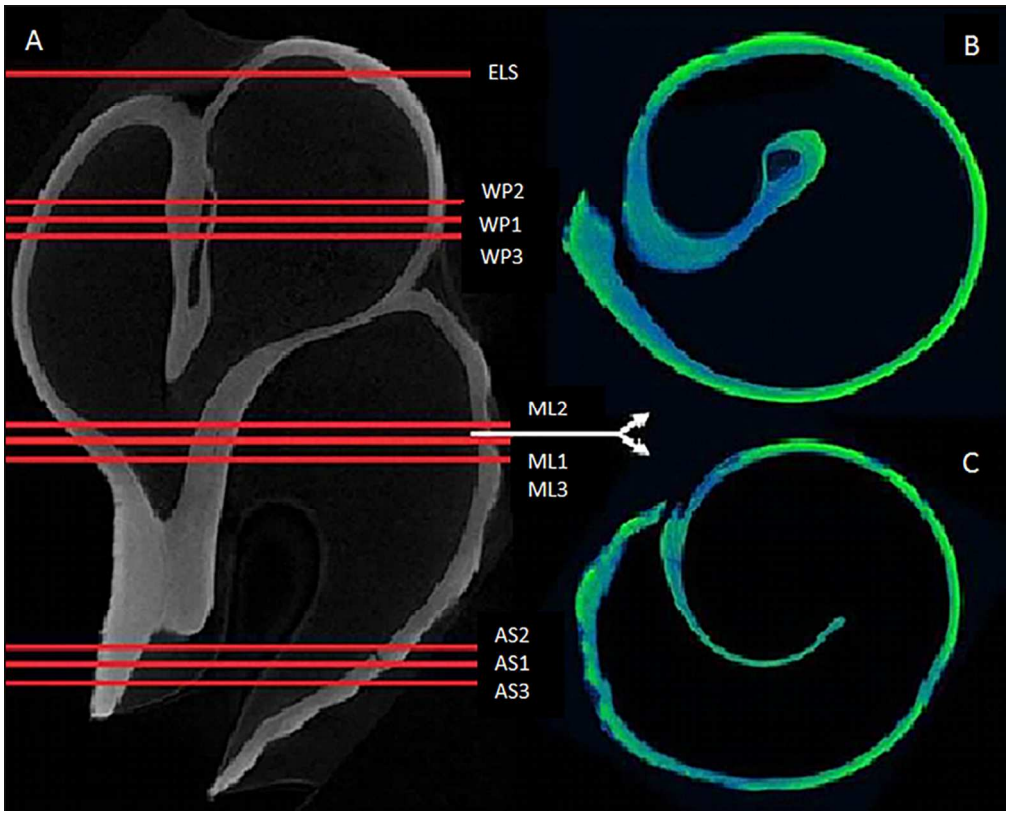

Figure 1: (A) Cross-sectional image of a nine week old Nucella shell taken with the micro-CT scanner, indicating the position of the horizontal shell slices used for analysis. ELS = 3 % from the top (posterior), AS1 = 3 % from the bottom (anterior), AS2 = 4 % from the bottom, AS3 = 5 % from the bottom, WP1 = Widest Point, WP2 = WP1+1 %, WP3 = WP1-1 %, ML1 = Mid-Lip, ML2 = Mid-Lip +1 %, ML3 = Mid-Lip -1 %. Lighter colour indicates higher shell density, while black illustrates the background medium (air), not included in the analysis. 1 (B) and (C) are horizontal slices which illustrate the differences in density throughout two randomly selected three week old shells. (B) is a shell from ambient conditions (380ppm CO2 / 9-15 °C), while (C) was exposed to elevated temperatures and CO2 input (750ppm CO2 / 9-15 +2 °C) . Colours represent densities: green: denser areas, blue: less dense areas.

85x68mm (300 x 300 DPI)

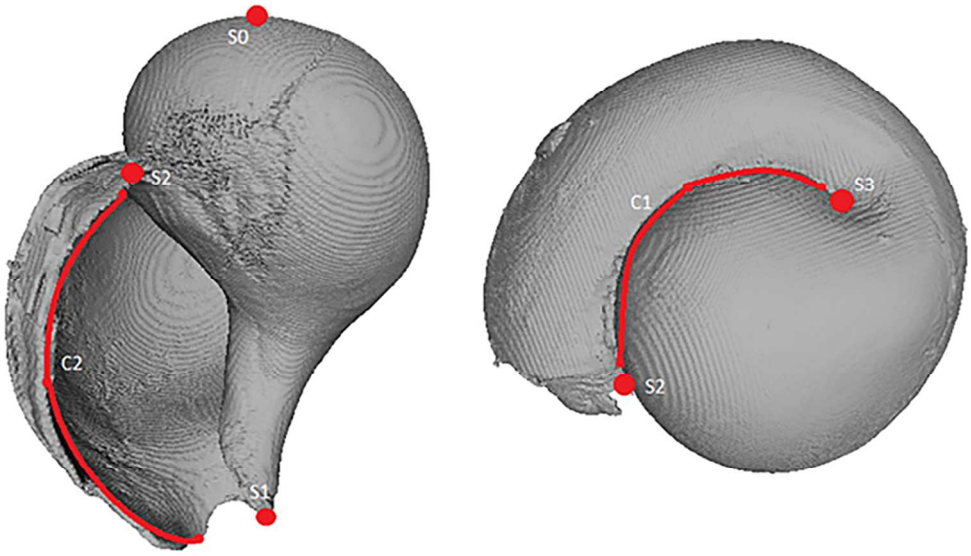

Figure 2: Surface model of a shell, reconstructed using μ-CT. The landmark protocol used in this study to evaluate shell morphology is represented by the red curves and dots. S0-S3 are single landmarks while C1 and C2 represent curves.

85x48mm (300 x 300 DPI)

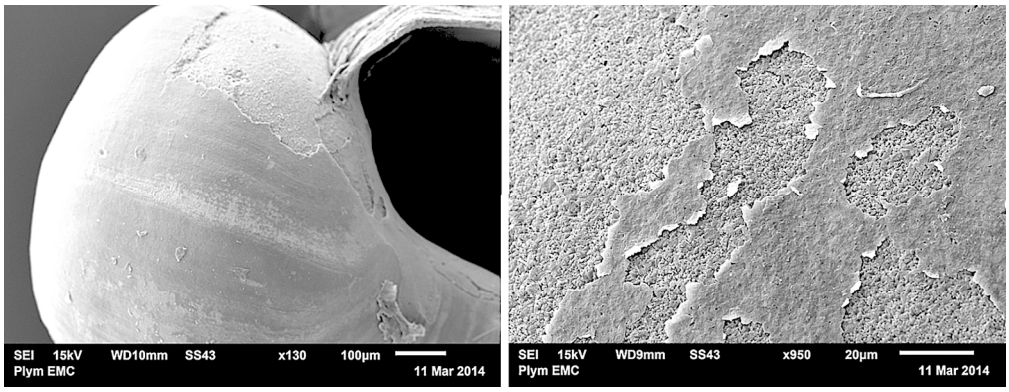

Figure 3: Images of shell exteriors taken with the electron microscope (EM) to show examples of surface damage in 750T (left) and 750A (right) shells.

170x64mm (300 x 300 DPI)

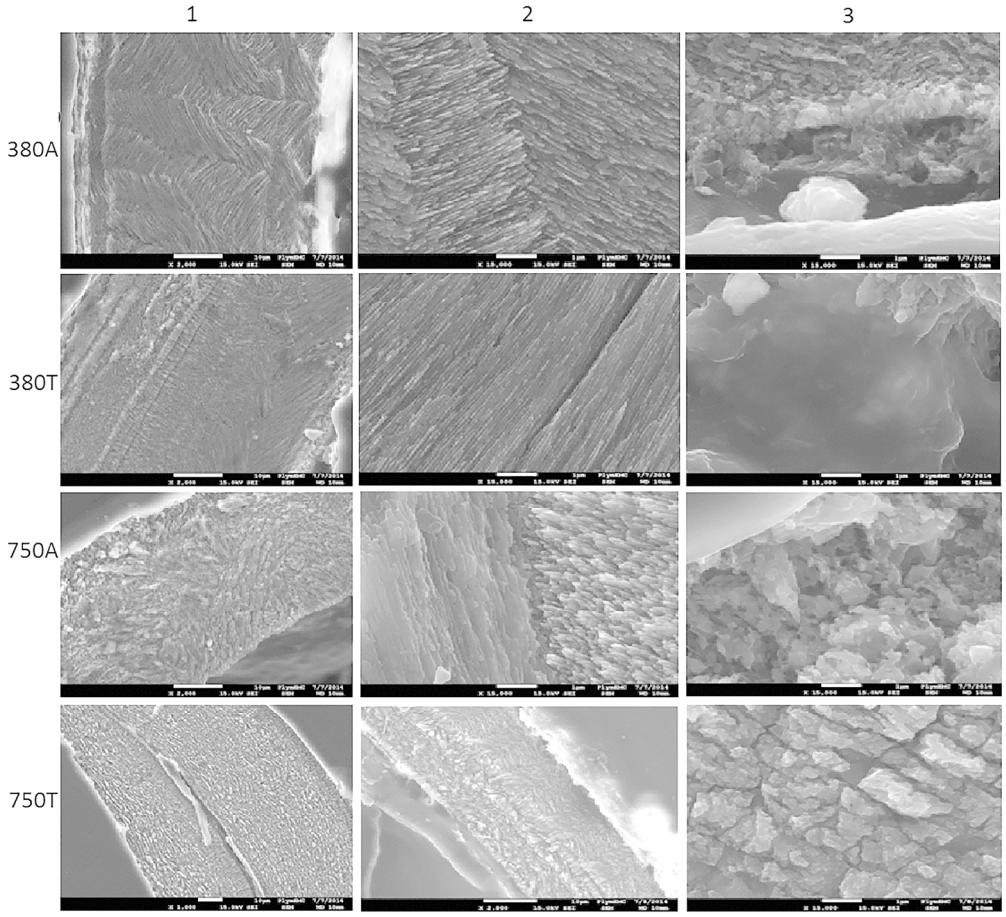

Figure 4: Electron microscopy images of the crystallised structures within shells of the older group in lines according to treatments; columns 1 represents a view of both layers together, 2 shows a close-up of the crossed-lamellar layer, and column 3 are images of the homogenous structures. The first picture depicting the 750T treatment represents a shell with no distinct difference between layers, the second in that line shows an example of a shell with remnants of crossed-lamellar structuring and the third picture is a close-up of the bark-like structure.

170x156mm (300 x 300 DPI)

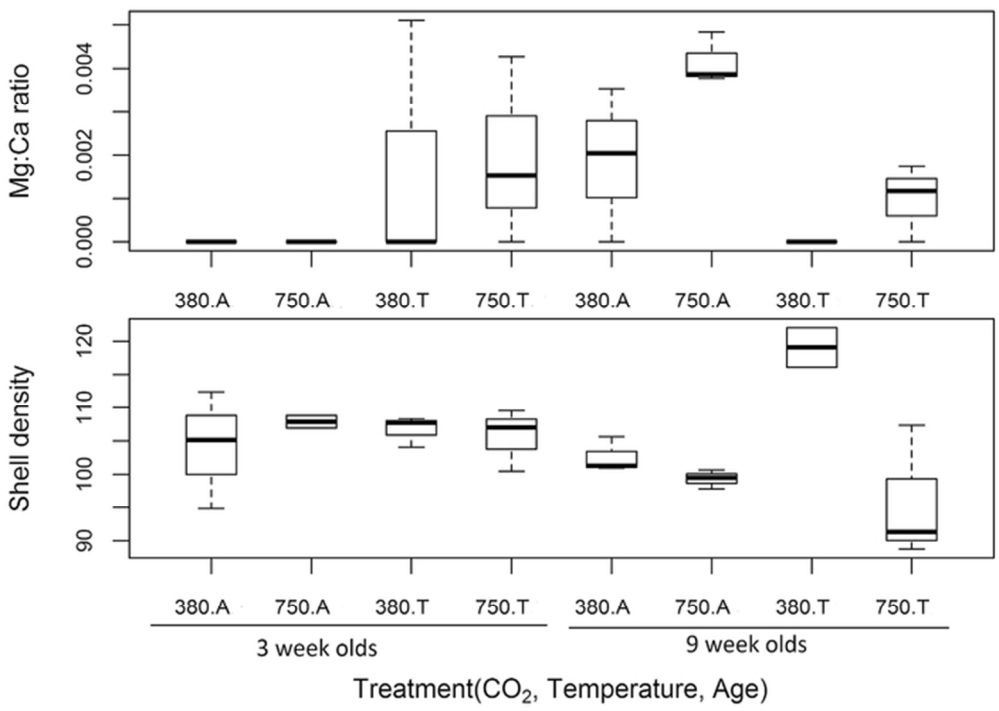

Figure 5: The effect of exposure to elevated pCO2 and temperature, in juveniles of N. lapillus of different age (weeks 3 and week 9 post exposure) on shell (A) Mg2+:Ca2+ ratios and (B) density which are coded along the x-axis with a combination of pCO2 content (380 or 750 µatm), temperature (A for ambient, T for elevated by 2 °C) and age (3 and 9 weeks).

59x42mm (300 x 300 DPI)

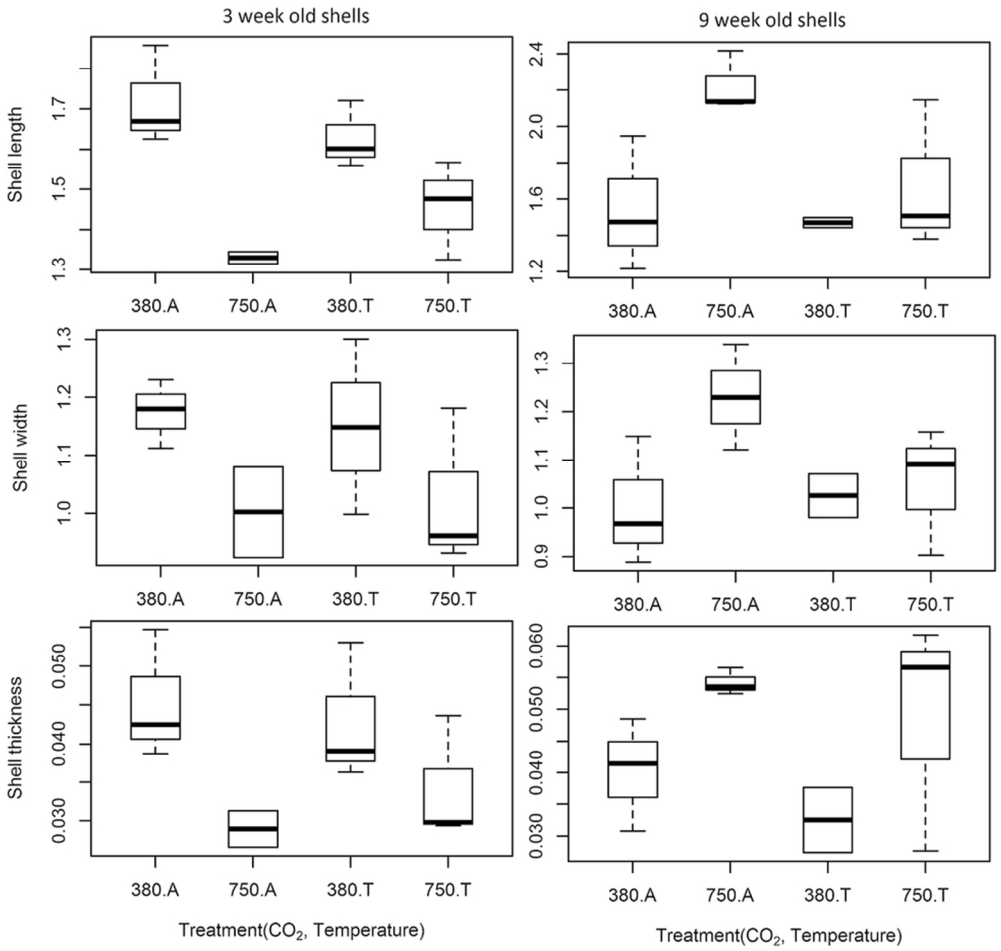

Figure 6: The effects of exposure to elevated pCO2 and temperature, in juveniles of N. lapillus of different age (weeks 3 and 9 post exposure) on shell (A) length, (B) width and (C) thickness which are coded along the x-axis with a combination of CO2 content (380 or 750), temperature (A for ambient, T for elevated) and age (3 and 9 weeks).

83x81mm (300 x 300 DPI)

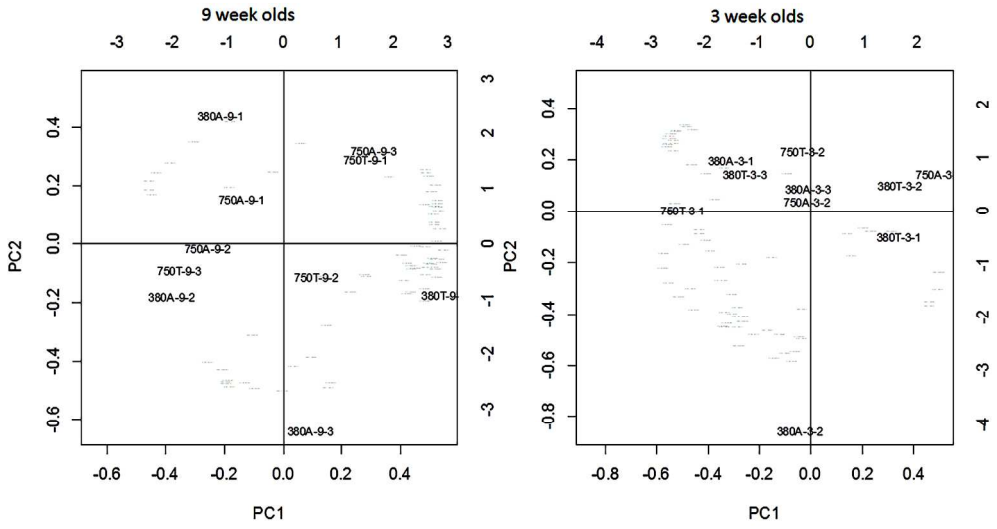

Figure 7: PC1 and PC2 of nine week old shells to the left (A) and three weeks old shells to the right (B)

170x88mm (300 x 300 DPI)

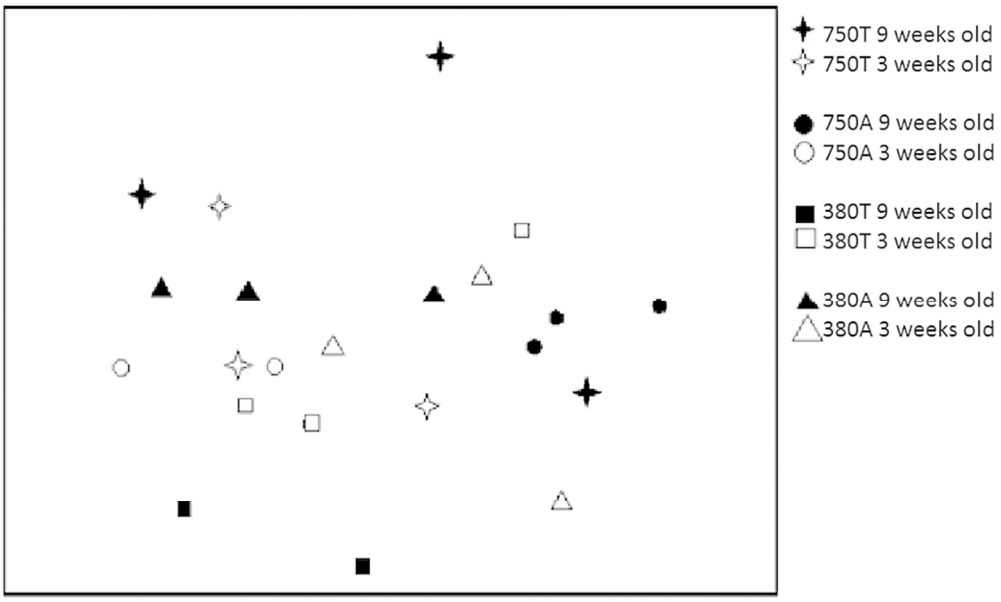

Figure 8: nMDS plot of similarities and dissimilarities between individuals according to age and treatment groups.

85x50mm (300 x 300 DPI)